Experimental Research on the Flow in the Steam Turbine Axial Exhaust Hood

David Tupy[1,*], *Vaclav* Slama[1], and *Robert* Kalista[1]

[1]Doosan Skoda Power, Experimental Research, Tylova 1/57, Pilsen, Czech Republic

Abstract. There is the still remaining task to increase the efficiency of power plants and steam turbines. One possibility to increase the thermodynamic efficiency is to apply a suitable exhaust hood. Axial exhaust hoods are mainly designed for small turbines up to 180 MW. They are a very important part of steam turbines and its main purpose is to take away the steam from the last stage outlet to a condenser with minimal loss or even with pressure compression and an increase in the last stage enthalpy drop. This paper concerns experimental measurements on the axial exhaust hood wind tunnel model. The main goal of this paper is to determine how given geometrical and flow parameters affect the resulting pressure recovery coefficient. Main observed parameters are velocity and circumferential angle profiles at the diffuser inlet along with a number, shape and geometrical configuration of internal struts. Several geometrical variants are measured for two types of circumferential angles at the diffuser inlet and for two values of Mach number in the presented work. Multi-hole pneumatic probes and pressure taps are used for flow parameters measurement. The proposed experimental model, along with corresponding CFD (computational fluid dynamics) simulations, will help to optimize the flow parameters in the exhaust hood and allow a decrease in pressure losses in this part.

1 Introduction

One reason to increase the power plant efficiency is to lower the amount of burned fuel and in this way also the operational costs. Another reason is the present trend to reduce harmful emissions. Thermodynamic efficiency can be increased by using a suitable exhaust hood. This paper deals with the experimental research of flow in the axial exhaust hood and optimization of its shape.

Axial exhaust hood are often used as a type of the steam turbine outlet. They are mainly used for turbines of lower outputs up to 180 MW, with the condensers located at the same height level. The axial exhaust hood 3D view is shown in Fig. 1.

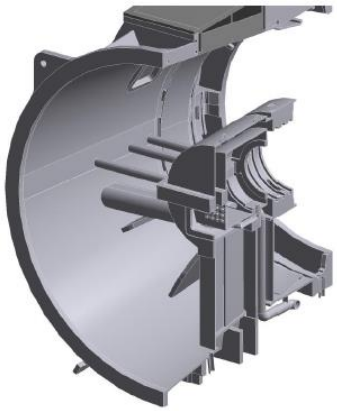

Fig. 1. Exhaust hood 3D view.

In comparison with radial hoods, the advantage of axial hoods is a simpler shape and thus also the construction and the related energy losses. Exhaust hoods are construction nodes of considerable dimensions in comparison with other turbine parts, which results in various designs and technological constraints. That is why exhaust hoods are made mainly as weldments with simple shape without much emphasis on aerodynamic properties. Condensing turbines operate at a condensing pressure which is substantially lower than the atmospheric pressure. In the case of axial hoods, among other things, there is a problem with static rigidity of the bearing stand that is surrounded by flowing water steam. For this reason it is necessary to produce hoods with various struts and supports to prevent the casting from collapsing due to external atmospheric pressure. A number of pipelines (oil, seal, regenerative) go very often through the exhaust hood and provide required performance characteristics. The mentioned inner elements form obstacles in the steam flow and generally have an adverse effect on pressure losses. However, these losses can be considerably reduced by a suitable choice of internal struts shape, size and configuration. It is also possible to reach uniformity of velocity field at the hood outlet that reduce unfavourable vibrations of pipe bundles in the condenser, even if in the case of axial exhaust hood the pipe bundle is located rather far from the exhaust hood. A detailed study of the influence of internal support in exhaust hood on its pressure recovery factor is presented in e.g. [1]. The main task of the

* Corresponding author: david.tupy@doosan.com

construction design is to delay or eliminate the occurrence of the boundary layer separation, which has a crucial impact on energy losses. There are also a number of measures that contribute to reducing energy losses, such as a boundary layer suction or, conversely, blowing steam into the boundary layer on the outer side of the diffuser.

The paper is devoted to an experimental verification of the flow on the scale model of the steam turbine axial exhaust hood. The main aim of the work was to define the influence of selected geometric and flow parameters on the c_p (pressure recovery coefficient). Among the observed parameters, there were the velocity profile at the exhaust hood inlet, the profile of circumferential angle α_1 at the exhaust hood inlet and the geometrical configuration of the exhaust hood internal struts. The paper deals with description of the experimental device, experimental verification of the flow, summary of methodology used and results obtained.

2 Experimental device

The experimental device is in fact a scale model of the air axial exhaust hood. The model is attached to the wind tunnel outlet, see Fig. 2. In the real machine it is very difficult to change the body geometry, arrangement of internal struts or to apply various experimental methods for flow research. For this reason a model of axial exhaust hood was made. On the other hand, in experimental conditions it is complicated to set the conditions at least close to the real operation. It is in fact impossible to reach an agreement. However, the results from experimental measurements are necessary for verification of the concurrently running numerical calculations. Using numerical calculations, it is possible to model states that cannot be reached in laboratory conditions, but with many simplifications due to limited computational capacities, see [2] and [3].

Fig. 2. Exhaust hood model with extension pipe.

The exhaust hood geometry represents a scale model corresponding to the real concept that was designed for the turbine with 35 MW output. The aerodynamic design of this scaled air test model of the axial exhaust hood is described in e.g. [4] and [5]. The steam turbine will be operated with the possibility of experimental verification of operational properties. Based on the available information it will be possible to compare data from the real machine and the air model. But it is not a part of this paper.

Mach number (Ma) is one of the key parameters characterizing the flow at the axial exhaust hood inlet. This parameter is considerably limited by the possibilities of the experimental laboratory mainly by the wind tunnel fan output. Experimentally, 0.4 Ma can be reached, while in the real machine the axial velocities reach minimally 0.5Ma. Nevertheless, the main task when designing the experimental model is to guarantee the required circumferential angle (α_1) of flowing medium at the exhaust hood inlet. The circumferential angle that changes along the inlet channel height (along the last rotor blade length) has a significant effect on the interaction between the flow and internal struts. In the real machine there is also a radial outlet angle of the flow that arises during the rotation of rotor blades of the steam turbine last stage. This angle is very hard to adjust on the testing device. For this reason the model was designed to achieve the required angles in the circumferential direction. The fact that the influences on the last stage output can be quite important is discussed in e.g. [6] and [7]. All together two types of a stator blade cascade were designed with circumferentially shaped blades. The first blade profile (Variant 1) is designed so that the required profile of the circumferential angle α_1 along the blade height is in agreement with the referential real machine. In the second case (Variant 2) 1.5 times the circumferential angle is achieved. In order to quantify the influence of the circumferential angle on the exhaust hood behaviour a blade cascade was designed with only the axial component of velocity (Variant 3). The required angle of the circumferential angle α_1 (the so called swirl angle) along the channel height for all three types of the blade cascade and the value of Mach number on the diffuser inlet 0.18 Ma can be seen in Fig. 3. Within this paper, only the results from Variant 1 and Variant 3 are presented.

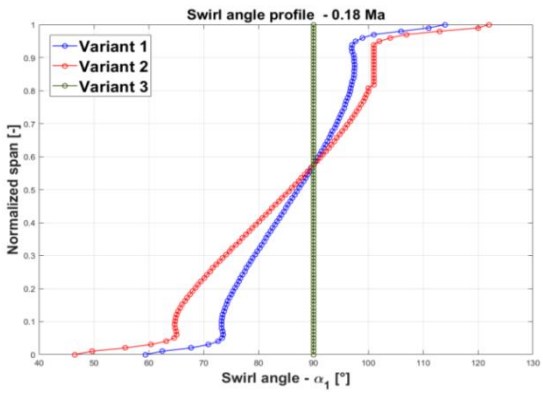

Fig. 3. Profile of circumferential angle α_1.

3 Measurement description

The exhaust hood diffuser consists of an annular and conical part. To the conical part an extension ring pipe is attached. In Fig. 4 a simplified scheme is shown with marked important plane:

- plane 0 – the plane upstream of the blade cascade,
- plane 1 – axial exhaust hood inlet ,
- plane 2 – axial exhaust hood outlet,
- plane 3 – extension pipe outlet into the open space.

Planes 0 and 1 are divided circumferentially into four measuring segments where it is possible to measure using multi hole pneumatic probes and a Prandtl probe. The segments are marked I to IV in the flow direction. It is possible to measure using pneumatic probes in the plane 1´, 1´´ and 2´. These planes are again divided around the perimeter into four measuring segments. In the plane – a, b, c, d, e static pressure taps are made. Due to the taps it is possible to obtain information about static pressure values in several planes along the exhaust hood length. On the exhaust hood, two temperatures are measured. The first one is taken in the wind tunnel settling chamber and the second one is taken in the plane upstream of the blade cascade (plane 0). For pressure measuring on the exhaust hood model pressure scanners NetScanner 9116 were used. Atmospheric pressure was measured using pressure transmitter Rosemount 3051S performance class ultra and temperatures were taken using resistance thermometers Pt100.

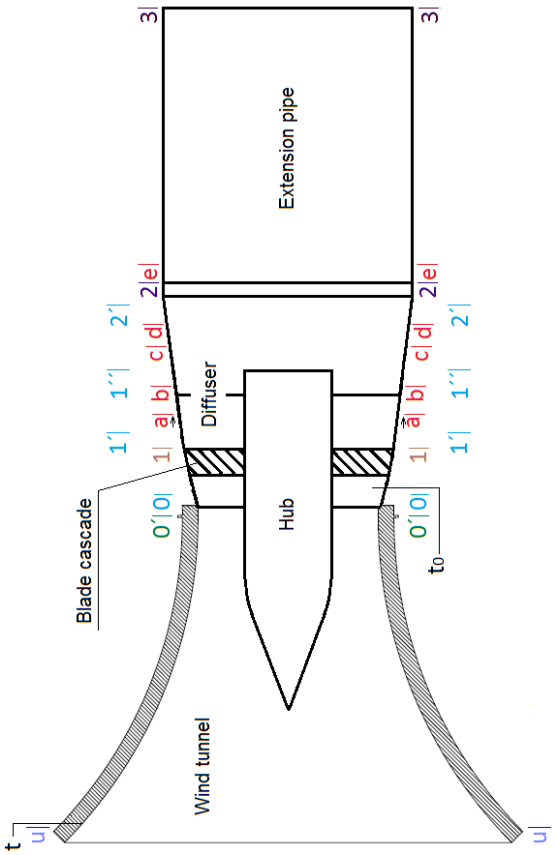

Fig. 4. Scheme with marked planes.

4 Data assessment

The ratio of dynamic pressures upstream and downstream of the blade cascade (p_p) and the loss coefficient of the cascade (ζ_m) are the most important parameters of stator blade cascade characteristics. In order to define these parameters it is necessary to measure in detail the blade cascade using traversing by pneumatic probes. The obtained parameters are then used as constants in equations for the evaluation of the so-called simple measurement when the pneumatic probe is placed in only one characteristic location of the flow field at the blade cascade inlet. Due to measurements in a simple mode the time consuming probe traversing is eliminated. The blade cascade is located at the inlet of the exhaust hood. Data are collected using multi hole pneumatic probes upstream and downstream the blade cascade. In the equations below there are the respective total pressures - p_c, static pressures - p_s and dynamic pressures - p_d. Parameters of the cascade are defined using the following equations:

$$\zeta_m = \frac{p_{c0} - p_{c1}}{p_{d0}}, \tag{1}$$

$$p_p = \frac{p_{d0}}{p_{d1}}. \tag{2}$$

One of the main tasks of the work was to define loss (ζ_D), or pressure recovery coefficient of the diffuser (c_{p_D}). The loss coefficient of the diffuser can be defined for incompressible flow using the following relation:

$$\zeta_D = \left(\frac{p_{c0} - p_{s2}}{p_{d0}} - \zeta_m\right) \cdot \frac{p_{d0}}{p_{d1}} = \\ = (\zeta_{mD} - \zeta_m) \cdot p_p. \tag{3}$$

Pressure recovery coefficient can be then defined using the relation:

$$c_{p_D} = 1 - \zeta_D. \tag{4}$$

Loss coefficient of the diffuser and the extension ring pipe (ζ_C) can be calculated for incompressible flow using the relation:

$$\zeta_C = \left(\frac{p_{c0}}{p_{d0}} - \zeta_m\right) \cdot \frac{p_{d0}}{p_{d1}} = \\ = (\zeta_{mC} - \zeta_m) \cdot p_p. \tag{5}$$

Pressure recovery coefficient can be then defined using relation:

$$c_{p_C} = 1 - \zeta_C. \tag{6}$$

For the calculation of both equations it is necessary to know the mean values of blade cascade parameters. For the purpose of this paper the blade cascade parameters were weighted by mass flow. Then the blade cascade parameters are marked - $\bar{\zeta}_m$ and $\bar{p}_p$.

Using static pressure taps it is possible to calculate the loss coefficient and pressure recovery coefficient also in other planes of the exhaust hood, i.e. in plane: a, b, c, d, e, see Fig. 4. Then it is possible to define the dependence of c_p in individual investigated planes on the relative distance of the planes from the trailing edge of the blades. The pressure recovery coefficient on the trailing edge of the blades is zero and gradually increases towards the outlet.

5 Numerical model

The package of ANSYS software tools was used to carry out required CFD analyses. The model consists of three parts: the inlet part which contains the inlet confusor, the middle part which contains the blade cascade and the outlet part which contains the investigated diffuser. Each section can be changed according to the investigated variant. The whole numerical model is shown in Fig. 5, the detail is in Fig. 6. The model is not symmetric due to different variants of the diffuser internal struts. Therefore, the model has to be complex without using a rotational periodicity.

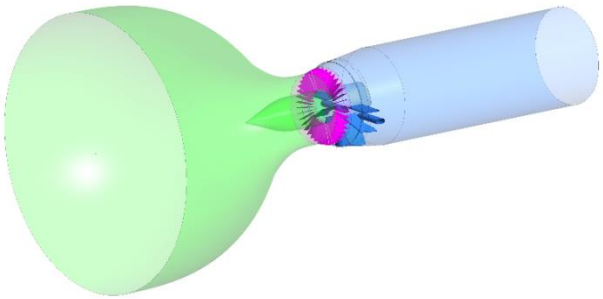

Fig. 5. Numerical model (the inlet part – green, the middle part – pink, the outlet part – blue).

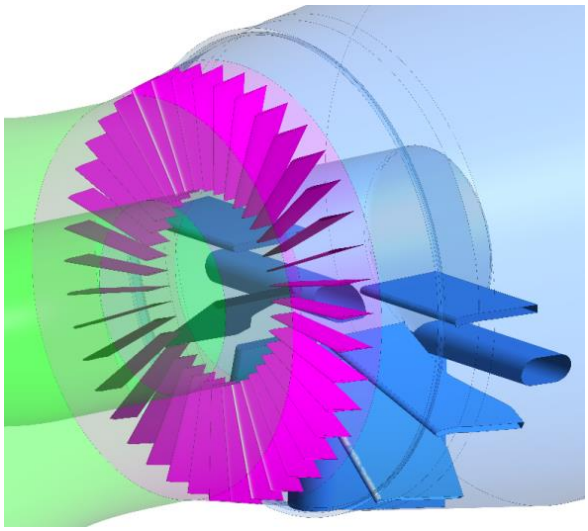

Fig. 6. Detail of the numerical model (the middle part with the blade cascade and the outlet part with diffuser internal struts).

ANSYS ICEM 18.2 and ANSYS Turbogrid 18.2 tools were used to create a fully structured hexahedral mesh for the inlet and middle part and a hex-core mesh for the outlet diffuser part. The picture of the hexahedral mesh is shown in Fig. 7, the hex-core mesh is shown in the cross section of the diffuser part in Fig. 8. The boundary layer with a 0.001 mm thickness of the first cell was created in all mesh parts and all mesh densities in order to keep the value of y+ lower than 5. In order to find the reasonable mesh density, a mesh sensitivity analysis was carried out. For this purpose, the global number of mesh nodes was changed. For the sake of simplicity, it is described by a size factor which is shown in Table 1 along with other details.

Table 1. Mesh sensitivity analysis: different mesh densities presented by mesh nodes (the outlet part is with all diffuser internal struts).

Number of nodes	Coarse	Medium	Fine
Size factor	0.25	0.50	1.00
Inlet part	298 973	936 000	1 872 000
Middle part	4 069 440	16 170 440	46 875 400
Outlet part	1 579 478	4 944 899	9 889 798
Total	5 947 891	22 051 339	58 637 198

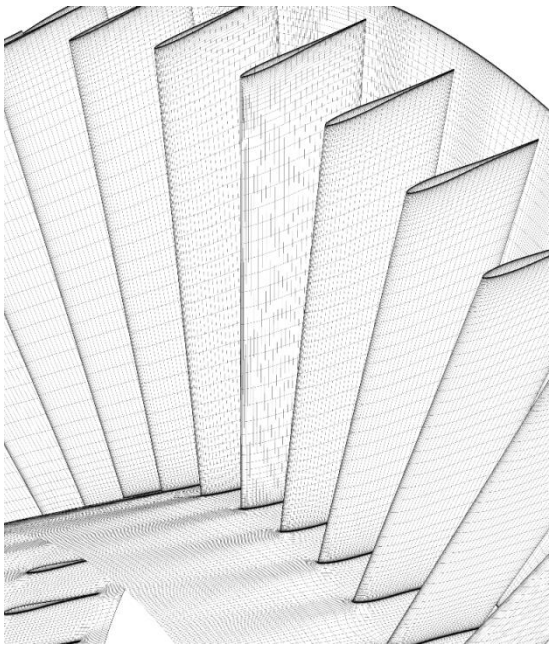

Fig. 7. Detail of the hexahedral mesh of the middle section.

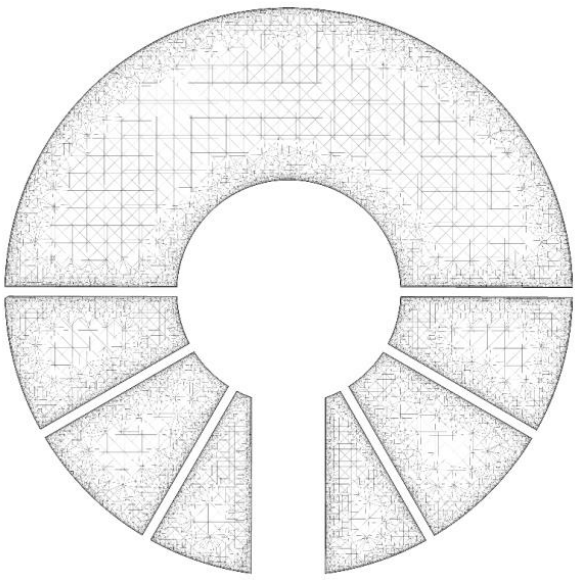

Fig. 8. Detail of the hex-core mesh in the cross-section through the outlet part.

In order to evaluate the mesh density influence, the integral values of c_p were compared for nominal boundary conditions of the test rig. As it can be seen in Table 2, the c_p result when using medium dense mesh is not so different from the fine mesh. As a result, the medium coarse mesh was chosen to be used for all the numerical analyses of different diffuser variants.

Table 2. Static pressure recovery factor depending on mesh densities.

Mesh density	Coarse	Medium	Fine
c_p (at position L = 0.44)	0.5710	0.4434	0.4429
Difference from the medium mesh [%]	28.8	0.0	-0.1

The solver ANSYS CFX 18.2 was used to carry out the numerical computations. This solver provides the steady state RANS (Reynolds-Averaged Navier-Stokes) solution with a compressible turbulent model. The k-ω SST turbulent model whose fidelity was validated in many prior Doosan Skoda Power projects using numerical and experimental results comparison was used. The medium was air which was defined as an ideal gas. A high resolution scheme was used to deal with the advection term and the turbulence numeric. A total pressure and a static temperature were defined at the domain inlet and a static pressure was defined at the outlet according to measurement results. The connections between the domains were defined as interfaces with a general connection.

Residual values and global imbalances were used to quantify simulation convergence criteria. The RMS (root mean square) residual type was chosen and 10^{-4} residual target value was defined. The global imbalances were less than 0.01 %. The values of required c_p were also monitored during each simulation in order to check that its convergence is appropriate.

6 Measured variants and results obtained

6.1 Blade cascade parameters - traversing mode

Loss coefficient of the cascade (ζ_m) and the ratio of dynamic pressures (p_p) upstream and downstream the blade cascade are characteristic parameters of the blade cascade. Within this paper four segments were measured on both variants of stationary blade cascade (Variant 1 and 3) for the value of Mach number 0.2 and 0.4 at the diffuser inlet (plane 1). The circumferential angle of each segment was chosen 27 °. This size of the angle enables to traverse over three blades of the cascade and in this way it is possible to adequately capture the vortex that arise behind the trailing edge of the blades. First, it was necessary to establish an appropriate procedure for data collecting. All together two types of measuring mesh were examined, the fine one and the coarse one. The fine mesh is formed by 324 points. For this type of mesh it was traversed along the channel height from 10 to 115 mm with the step of 10 mm (the last step was only 5 mm) and in the circumferential direction it was traversed by 1 °. In each point 100 readings were taken of 20 Hz frequency. This mesh measuring was very time consuming. For this reason then the coarse mesh was measured. The coarse mesh is made by 112 points. In each point again 100 readings were taken of 20 Hz frequency. For this type of mesh it was traversed along the channel height from 10 to 115 mm with the step of 15 mm and in the circumferential direction by 2 °. The coarse mesh can be seen in Fig. 9.

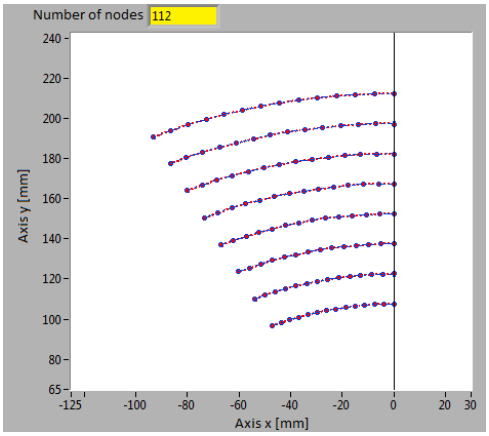

Fig. 9. Coarse mesh.

In order to verify the influence of the extension pipe even the variant without the extension pipe was measured. Measurements were carried out on the right upper segment (in the flow direction) for 1300 rpm, which corresponds with about 0.2 Ma on the diffuser inlet. The obtained results are arranged in Table 3. In the table the loss coefficient value and the ratio of pressures for simple average (Sa) and average weighted by mass flow (Mf) are shown.

Table 3. Mesh comparison – Variant 1 (0.2 Ma).

	Variant 1 – coarse mesh without pipe		Variant 1 – coarse mesh with pipe		Variant 1 – fine mesh with pipe	
	Sa	Mf	Sa	Mf	Sa	Mf
ζ_m	0.036	0.032	0.030	0.026	0.028	0.025
p_p	1.598	1.589	1.588	1.579	1.587	1.579

From the table it is evident that an extension of the hood has certain influence. For this reason, all the segments were measured with ring pipes fitted. The differences between the fine and coarse mesh with the ring extension pipe are practically negligible. Due to the time consumption of the fine mesh measuring the variant with coarse mesh was chosen.

The distribution of loss coefficient for Variant 1 and 0.2 Ma at the inlet can be seen in Fig. 10. From the picture it is evident that the loss coefficient reaches the highest value at the root diameter of the blade. This is

where the biggest losses occur. It can be also observed that a significant increase of loss coefficient occurs behind the trailing edge of the blades where also the emerging floods are present. From the picture it is also evident that the loss coefficient value in the right half is slightly higher than the loss coefficient in the left half. Considering this fact it is always suitable to measure several segments distributed over the entire space.

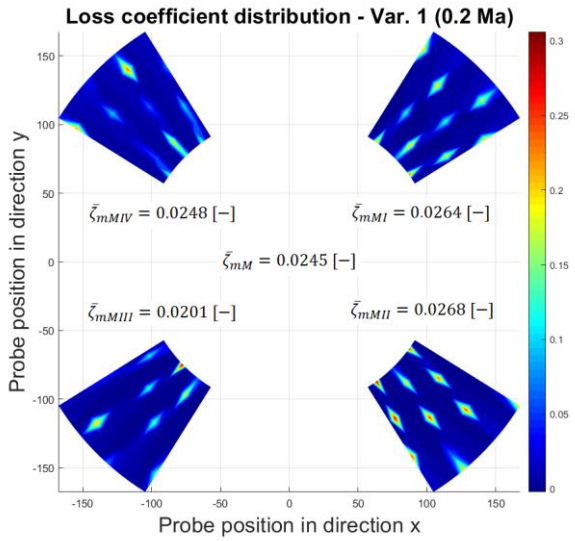

Fig. 10. Loss coefficient distribution.

The values of blade cascade parameters weighted by mass flow are given for individual variants in Table 4. From the table it is evident that the loss coefficient decreases with the increasing Ma value at the inlet. The loss of the blade cascade that models only the axial part of velocity (Variant 3) is approximately the same as for the cascade with circumferential shaped blades (Variant 1).

Table 4. Blade cascade parameters.

	Variant 1		Variant 3	
	0.2 Ma	0.4 Ma	0.2 Ma	0.4 Ma
$\bar{\zeta}_{mM}$	0.025	0.017	0.027	0.016
$\bar{p}_{pM}$	1.574	1.539	1.419	1.407

For illustration purposes, the profile of the swirl angle α_1 was plotted along channel height for several radials. Individual radials correspond with circumferential angle 32 °, 42 °, 50 ° and 58 °. For the sake of a comparison the results from CFD calculations was plotted as well and there is an obvious agreement between the results obtained from CFD calculations and those from the experiment. The blade cascade is for Variant 3 prismatic. In this case the flow does not curve along the blade height and the curvature angle at diffuser inlet reaches $\alpha_1 \cong 90$ °, see Fig. 11 - upper part. In Variant 1 the flow curvature can be seen with the inflection point at about 2/3 of the blade height, see Fig. 11- lower part. The courses are similar for both level of Mach number.

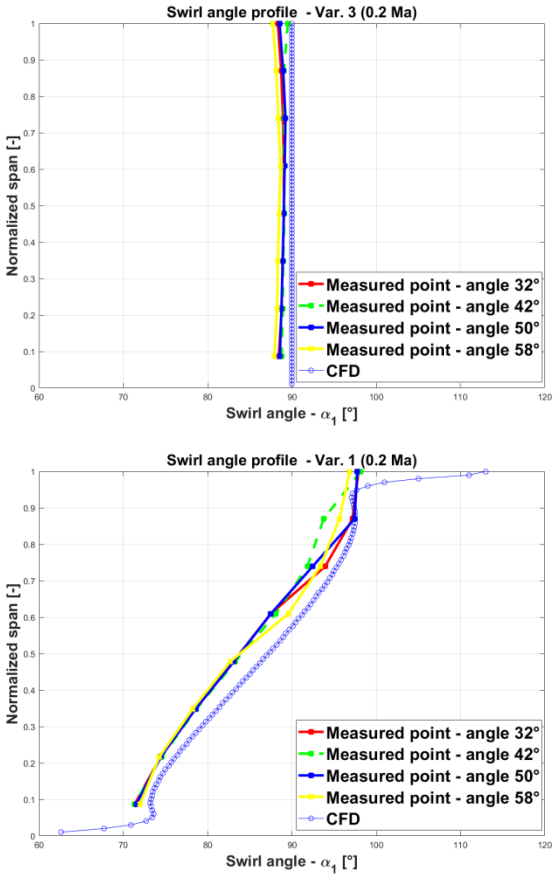

Fig. 11. Profile of swirl angle α_1 along the channel height.

6.2 Simple mode

Based on the knowledge of characteristic parameters of blade cascades of both variants and on verification of the circumferential angle distribution at the diffuser inlet it was possible to perform further measurements in the simple mode. During the measurements in the simple mode the Prandtl probe was located in the corresponding referential position. All together 6 variants were measured for each blade cascade for both Ma levels at the diffuser inlet.

6.2.1 Reference variant

The exhaust hood with the extension pipe without internal struts is considered as a reference variant. Pressure recovery coefficient values are given in Table 5. It is evident that in Variant 3 with increasing Ma value at the inlet the pressure recovery coefficient decreases, while in Variant 1 it in fact remains the same. As mentioned above, the prismatic blade cascade only derives the axial component of velocity and thus it is valid that $\alpha_1 = 90$ °. From the results, it is evident that the circumferential angle of the flow curvature at the exhaust hood inlet has certain influence on the final c_p. However, not as it was expected in a case of the hood with internal struts. The transition of the entering flow kinetic energy into pressure energy is between 67.2 to 73.8 %. The theoretical maximum value of pressure

recovery coefficient (c_p) is often stated, which can be defined using the relation:

$$c_{p_{max}} = 1 - \frac{1}{\left(\frac{S_2}{S_1}\right)^2}, \quad (7)$$

where:

S_1 - axial exhaust hood inlet cross section,

S_2 - axial exhaust hood outlet cross section.

The theoretical maximum value of c_p is 0.74 for the given ratio of cross section. Then, the exhaust hood losses for all reference variants are between 0.002 and 0.068, which are very good values.

Table 5. Pressure recovery coefficient values – reference variant.

	Variant 1		Variant 3	
	0.2 Ma	0.4 Ma	0.2 Ma	0.4 Ma
$c_{p,ref}$ [-]	0.674	0.672	0.738	0.699

The dependence of c_p on the length L of the exhaust hood supplemented by the ring extension pipe can be observed in Fig. 12. The black vertical line indicates the end of the exhaust hood. From the picture it is obvious that c_p increases along its entire length. The steepest increase is at the beginning of the hood. This increase corresponds with the sharp increase of static pressure caused by a large initial opening angle. The pressure recovery coefficient in the cone diffuser and ring pipe increases more slightly.

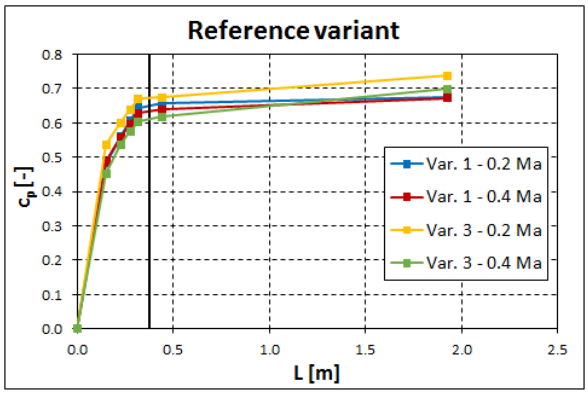

Fig. 12. Dependence c_p on L – reference variant.

Based on the knowledge of boundary conditions it was possible to perform CFD calculations and to compare the obtained results with experimental measurements. In Fig. 13 it is possible to observe the dependence of c_p on the length L for Variant 1 (0.2 Ma). Trends of both curves are similar. However, there is a certain difference between the obtained results.

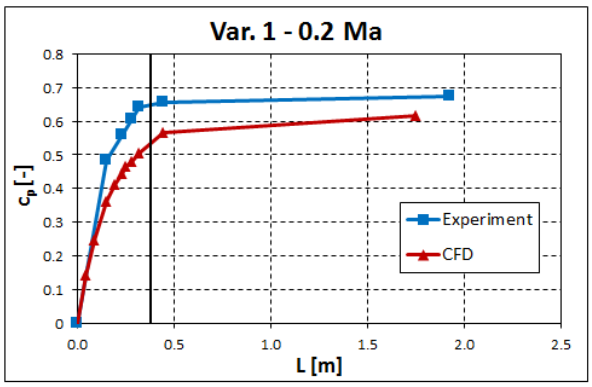

Fig. 13. Comparison of results – reference variant.

This difference is partly caused by the measurement in the simple mode. The traversing mode is a detailed process and the results of this type of measurement are reliable. Due to time constraints it is not possible to verify all variants using the traversing mode, and thus measurement in the simple mode is used. All measured data must be transformed in a very complex process. Many regressions must be used for both the measurement in the centre of gravity of each element of the cascade and for defining the reference position. Subsequently, the probe is placed into an exact position in one chosen segment and it is assumed that the circumferential flow does not change much. Based on these simplifications there will be a certain deviation from the real values and it can make the difference between the results obtained from experimental measurements and the results from CFD calculations.

Pressure recovery coefficient values of the exhaust hood extension pipe obtained from measurements in the simple and traversing mode and the values obtained from CFD calculations are given in Table 5. It is evident that the difference between the traversing mode results and CFD calculations are smaller than the differences between the simple mode results and CFD calculations. For better illustration a bar chart was created that can be seen in Fig. 14.

Table 6. Comparison of pressure recovery coefficient values.

	Variant 1		Variant 3	
	0.2 Ma	0.4 Ma	0.2 Ma	0.4 Ma
Simple mode	0.674	0.672	0.738	0.699
Traversing mode	0.660	0.661	0.678	0.662
CFD	0.618	0.626	0.644	0.646
Simple mode - CFD	**0.056**	**0.046**	**0.094**	**0.053**
Traversing mode - CFD	**0.041**	**0.034**	**0.034**	**0.016**

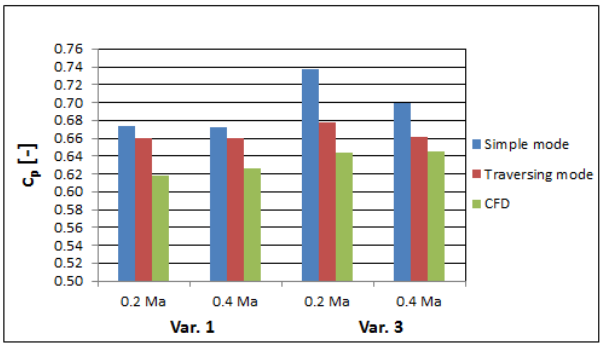

Fig. 14. Comparison of pressure recovery coefficient values.

Fig. 15 shows how the velocity profile develops in dependence on the length L for both measured variants with 0.2 Ma at the inlet. Gradually several radials were measured along the hood length in the plane 1, 1´, 1´´ and 2´ using a three hole pneumatic probe, see the scheme in Fig. 4. Radials were measured in the upper right segment (segment *I*). In the picture the exhaust hood is shown schematically. It is evident that towards the outlet the flow velocity is decreasing. Kinetic energy is transformed into pressure energy. In the last two planes it was traversed from the hood axis to the wall. However, behind the hub a considerable vortex occurs and the flow is here strongly turbulent. For this reason, it was possible to assess only the data taken at a certain distance from the centre of the channel.

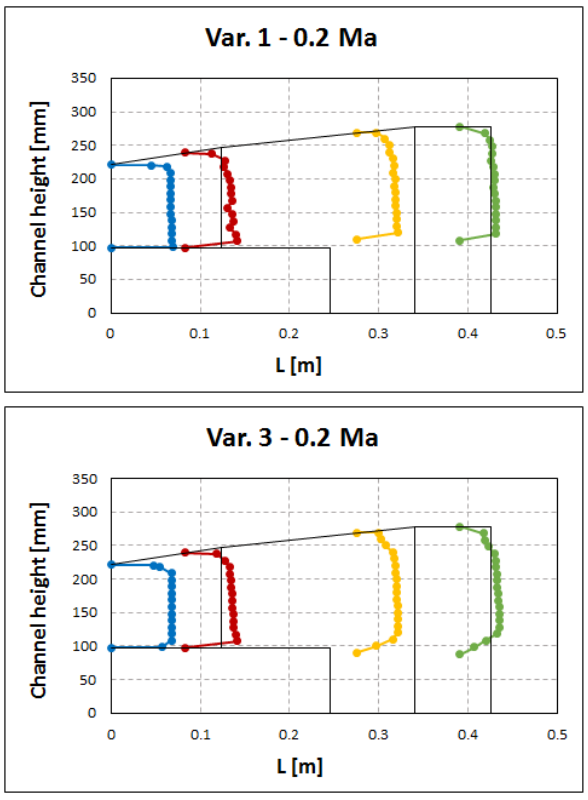

Fig. 15. Velocity profile in dependence on *L*.

6.2.2 *Variant with all struts – Variant e*

The location of individual struts can be seen in Fig. 16. All are located in the lower half of the hood. In Table 7 c_p values are given. For comparison also the values corresponding with the reference variant are presented here as well as the drop of c_p value. It is evident that the internal struts significantly influence the increase of loss coefficient values or the decrease of pressure recovery coefficient values. As a result, it is evident that the influence of Mach number on c_p is minimal for both variants of blade cascades.

Fig. 16. Variant with all struts – Variant e.

Table 7. Pressure recovery coefficient values – all struts.

	Variant 1		Variant 3	
	0.2 Ma	0.4 Ma	0.2 Ma	0.4 Ma
$c_{p,e}$ [-]	0.616	0.615	0.703	0.672
$c_{p,ref}$ [-]	0.674	0.672	0.738	0.699
Drop c_p [-]	**0.058**	**0.056**	**0.035**	**0.027**

In Fig. 17 the dependence can be seen of c_p on length L for an empty and full hood. (0.2 Ma). A similar trend can be reached also for the value 0.4 Ma at the inlet. The beginning and the ending of all struts is marked with black vertical lines. It can be seen that at the beginning the pressure recovery coefficient increases sharply for all variants. However, in the full hood the static pressure decreases significantly, which is caused by the struts. The struts reduce the cross section of the diffuser, which causes a local increase of flow velocity. The static pressure is restored and rising steeply in the remaining part of the diffuser. The pressure recovery coefficient in the ring pipe increases more slowly, which is given by a slight decrease of flow velocity.

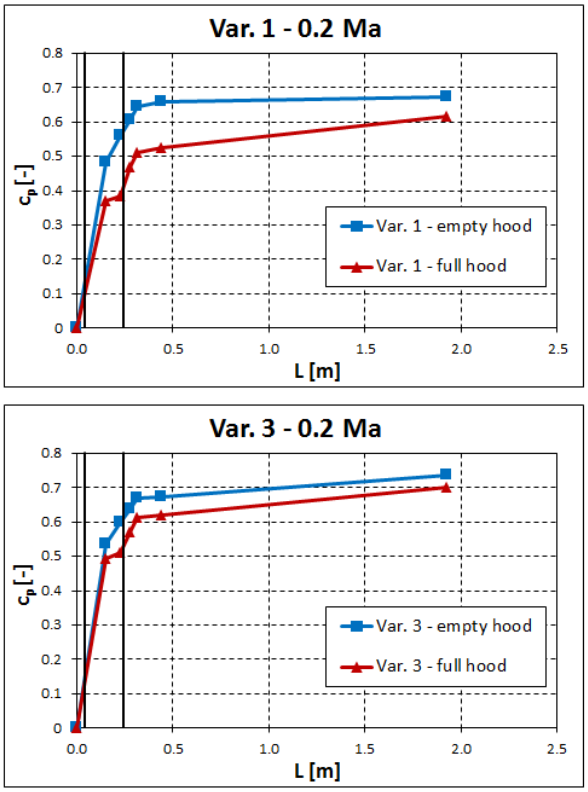

Fig. 17. Comparison of pressure recovery coefficient of the full and empty hood**.**

It is evident from the results that better results are obtained when the trailing angle of the flow into the strut is axial. For the curved blade cascade the flow entering the diffuser is curved too and thus the flow angle in the strut is not ideal. Due to poor flow around the internal struts larger energy losses occur, which is reflected in the increase of loss coefficient value. In order to reach higher values of c_p it is suitable to turn the struts, if possible, in the flow direction.

For the sake of comparison, the CFD calculations were carried out again. The trend of c_p along the length L for Variant 1 and 0.2 Ma can be seen in Fig. 18. Similar trend is reached for other measured variants.

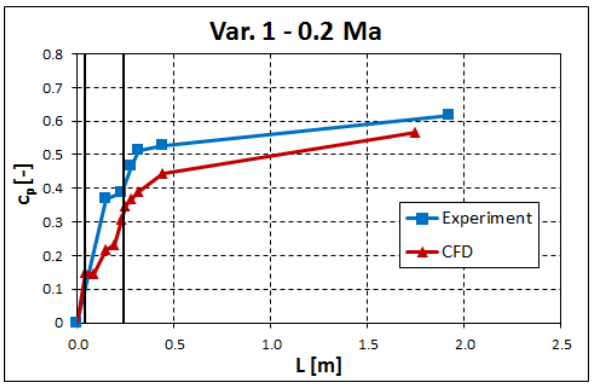

Fig. 18. Result comparison - full hood.

6.2.3 Other measured variants

Individual measured variants, locations of internal struts and variant labelling can be seen in Fig. 19. Measurements were carried out for both types of blade cascade and for both Ma values. As for the strength, only the variant with all struts is suitable, but in order to assess the influence of individual struts also the variants were measured with a lower number of internal struts.

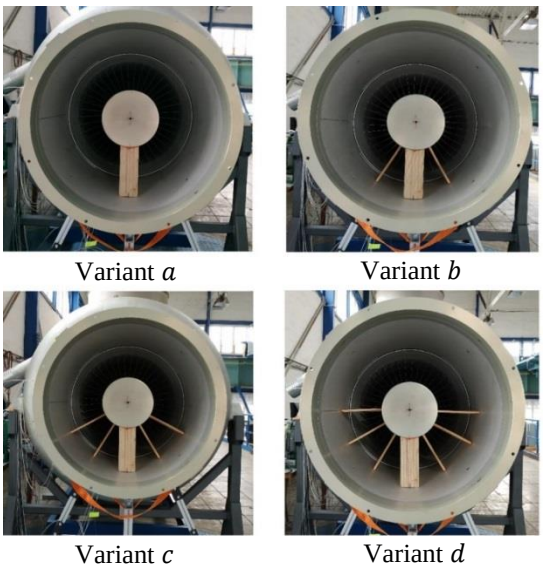

Fig. 19. Measured variants.

In Table 8 all values of c_p are shown for all measured variants. From the table it is evident that by adding each strut (pair of struts) a decrease of c_p arises compared to the previous variant. The only exception is adding the first pair of struts in Variant 3. In Fig. 20 it can be seen how c_p value drops with adding another strut (pair of struts). Based on this bar chart it can be defined which strut has the biggest influence on c_p value drop. For 0.2 Ma it is evident that inserting flat struts in the horizontal plane (Variant d) and traverse struts (Variant e, see Fig. 16) is the most influential. On the other hand for 0.4 Ma inserting bottom struts is most influential (Variant a). Conversely, inserting the first pair of flat struts (Variant b) participates minimally and for Variant 3 even an increase of c_p arises in comparison with the previous variant.

Table 8. Pressure recovery coefficient values.

	Variant 1		Variant 3	
	0.2 Ma	0.4 Ma	0.2 Ma	0.4 Ma
$c_{p,ref}$ [-]	0.6739	0.6716	0.7379	0.6993
$c_{p,a}$ [-]	0.6685	0.6538	0.7363	0.6871
$c_{p,b}$ [-]	0.6614	0.6536	0.7318	0.6889
$c_{p,c}$ [-]	0.6518	0.6445	0.7263	0.6874
$c_{p,d}$ [-]	0.6331	0.6299	0.7143	0.6816
$c_{p,e}$ [-]	0.6164	0.6153	0.7027	0.6718

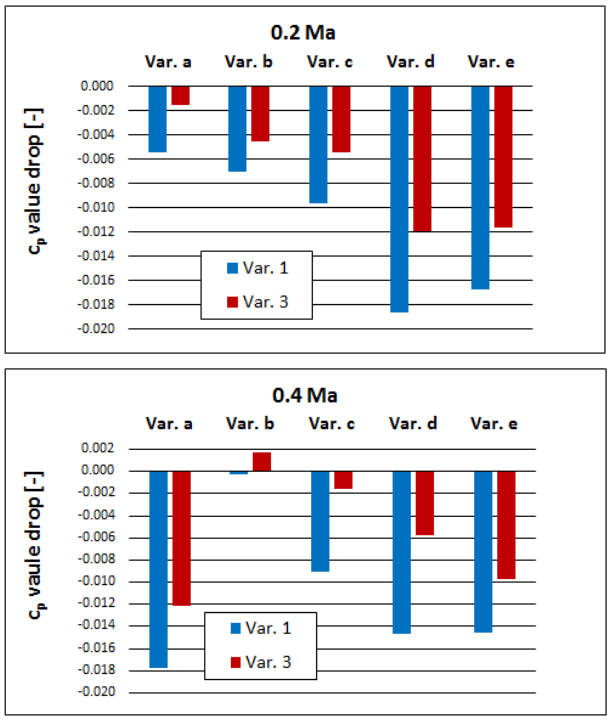

Fig. 20. Influence of individual struts.

For illustration the Variant c is compared here again (Variant 1 – 0.2 Ma). The dependence of c_p on the exhaust hood length is shown in Fig. 21. From the picture, an agreement is evident between experiment measurement results and CFD results.

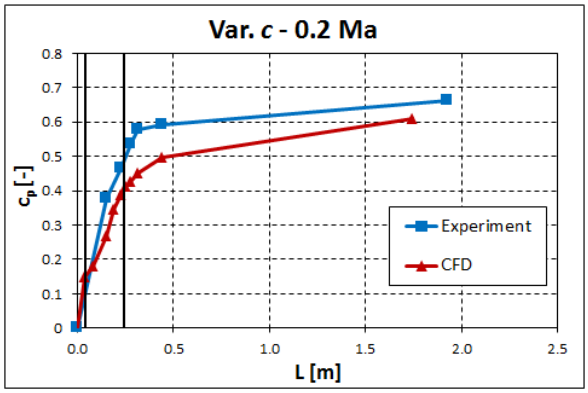

Fig. 21. Result comparison – Variant c.

7 Conclusion

The main aim of this paper was to define the pressure recovery coefficient (c_p) increase on the experimental model of the axial exhaust hood, the influence of the circumferential angle (α_1) and the influence of individual struts. The obtained results were compared to CFD calculations based on corresponding boundary conditions.

First of all, measurements were carried out for an empty hood variant. Then, the hood was fitted with various internal struts and their influence on c_p was evaluated. Measurement was carried out for two variants of the circumferential angle at the diffuser inlet and two levels of Mach number at the diffuser inlet, namely 0.2 and 0.4 Ma. The required inlet angle was defined by circumferentially shaped stator blades. The first blade profile (Variant 1) was designed so that the required angle was in agreement with a real turbine. The second blade profile (Variant 3) was designed with only the axial velocity component, which made it possible to describe the influence of the flow circumferential angle on the exhaust hood behaviour.

The first important part of the paper was to define characteristic parameters of the blade cascade, namely the cascade loss coefficient (ζ_m) and the ratio of dynamic pressures (p_p). In order to define these parameters it was necessary to measure several segments along the perimeter in the traversing mode. Based on the knowledge of blade cascade parameters it was possible to continue the measurements in the simple mode and in this way to define c_p in an empty hood which ranges for particular variants from 0.672 to 0.738. As a result, it is evident that about 70 % of kinetic energy of the flow is transformed into pressure energy. For the given ratio of cross sections the maximal pressure recovery coefficient is 0.74. Then, the exhaust hood losses for all reference variants (empty exhaust hood) are between 0.002 and 0.068, which are very good values. Consequently, measurements were carried out with individual variants of internal struts. The presence of struts had in all cases a negative impact on c_p compared to the reference variant. In Variant 1, adding the third pair of flat struts had the biggest impact on c_p (Variant d). In variant 3, the biggest impact on c_p was measured for bottom strut location (Variant a). Due to the strength only the variant with all internal struts is suitable (Variant e). Compared to the reference variant, in Variant 1 the decrease was by about 0.058 and in Variant 3 by about 0.03. From this result, it is evident that the circumferential angle negatively contributes to the pressure recovery coefficient for the full hood. It is caused by different behaviour of the flow behind the blade cascade and thus flow running around the struts is different for both cases.

Based on pressure recovery coefficient trend along the exhaust hood length it can be seen that most kinetic energy is transformed into pressure energy at the beginning of the hood. For this reason it is recommended to place the struts as far as possible from the trailing edges of the last rotor blades. From the results the negative impact of internal struts on c_p also evident and therefore it is advantageous to insert as few struts as possible. If possible, it is suitable to turn the struts in the flow direction, see the circumferential angle influence and the flow entering the struts.

The results and knowledge obtained can be transferred to CFD calculations which can be thus refined. The aim is to achieve a certain universal procedure in determining the pressure recovery coefficient of the exhaust hood so that it would not be necessary to perform experiment measurements for each type of the hood.

Acknowledgement

The authors of the paper would like to thank TAČR project Zéta TJ01000048 „Lowering outlet losses in steam turbines of modern construction“ and project "LoStr" no. CZ.02.1.01/0.0/0.0/16_026/0008389 for financial support.

Reference

1. R. Kalista at al., *The experimental investigation of the internal support effects on exhaust casing pressure recovery*, ASME IMECE 2017, IMECE2017-70279, Tampa, USA, (November 2017).
2. J. Fu, J. Liu, *Investigation of Influential Factors on the Aerodynamic Performance of a Steam Turbine Exhaust Systém*, In proceedings of ASME Turbo Expo. GT2010-22316, (2010).
3. A. Hirschmann, S. Volkmer, M. Schatz, C. Finzel, M. Casey, *The influence of the Total Pressure Profile on the Performance of Axial Gas Turbine Diffusers*, In Proceedings of ASME Turbo Expo. GT2010-22481, (2010).
4. R. Kalista, L. Mrozek,V. Slama at al., *Experimental measurement on the air test rig of the axial steam turbine exhaust casing*, AIP Conference Proceedings 2047, 020006 (2018).
5. R. Kalista at al., *Experimental and numerical design of axial exhaust diffuser test rig for investigation the aerodynamic performance of steam turbine and its enhancement by shape modifications*, ASME Turbo Expo 2019, GT2019-91313, Phoenix, Arizona USA, (June 2019).
6. M. Hoznedl at al., *The pressure field at the output from a low pressure exhaust hood and condenser neck of the 1090 MW steam turbine – experimental and numerical research*, ASME Turbo Expo 2018, GT2018-75248, Oslo, Norway, (June 2018).
7. M. Hoznedl, et al., *Experimental Investigation on Flow in Diffuser of 1090 MW Steam Turbine*, Proc. XX. International Conference The Application of Experimental and Numerical Methods in Fluid Mechanics and Energy, (2016).